AFRL-RX-WP-TP-2009-4051

NANOSCALE CHARACTERIZATION OF ELEMENTAL PARTITIONING BETWEEN GAMMA AND GAMMA PRIME PHASES IN RENE 88DT NICKEL BASE SUPERALLOY (PREPRINT)

J. Tiley, J.Y. Hwang, R. Banerjee, R. Srinivasan, G.B. Viswanathan, and H.L. Fraser

Metals Branch
Metals, Ceramics and NDE Division

FEBRUARY 2008

AIR FORCE RESEARCH LABORATORY
MATERIALS AND MANUFACTURING DIRECTORATE
WRIGHT-PATTERSON AIR FORCE BASE, OH 45433-7750
AIR FORCE MATERIEL COMMAND
UNITED STATES AIR FORCE

REPORT DOCUMENTATION PAGE

Form Approved
OMB No. 0704-0188

1. REPORT DATE *(DD-MM-YY)*	2. REPORT TYPE	3. DATES COVERED *(From - To)*
February 2008	Journal Article Preprint	

4. TITLE AND SUBTITLE

NANOSCALE CHARACTERIZATION OF ELEMENTAL PARTITIONING BETWEEN GAMMA AND GAMMA PRIME PHASES IN RENE 88DT NICKEL BASE SUPERALLOY (PREPRINT)

5a. CONTRACT NUMBER
In-house

5b. GRANT NUMBER

5c. PROGRAM ELEMENT NUMBER
62102F

6. AUTHOR(S)

J. Tiley (AFRL/RXLMD)
J.Y. Hwang and R. Banerjee (University of North Texas)
R. Srinivasan, G.B. Viswanathan and H.L. Fraser (The Ohio State University)

5d. PROJECT NUMBER
4347

5e. TASK NUMBER
RG

5f. WORK UNIT NUMBER
M02R1000

7. PERFORMING ORGANIZATION NAME(S) AND ADDRESS(ES)

Metals Branch (RXLMD)
Metals, Ceramics and NDE Division
Materials and Manufacturing Directorate
Wright-Patterson Air Force Base, OH 45433-7750
Air Force Materiel Command, United States Air Force

Department of Materials Science and Engineering
University of North Texas
Denton, TX

Department of Materials Science and Engineering
The Ohio State University
Columbus, OH

8. PERFORMING ORGANIZATION REPORT NUMBER

AFRL-RX-WP-TP-2009-4051

9. SPONSORING/MONITORING AGENCY NAME(S) AND ADDRESS(ES)

Air Force Research Laboratory
Materials and Manufacturing Directorate
Wright-Patterson Air Force Base, OH 45433-7750
Air Force Materiel Command
United States Air Force

10. SPONSORING/MONITORING AGENCY ACRONYM(S)

AFRL/RXLMD

11. SPONSORING/MONITORING AGENCY REPORT NUMBER(S)

AFRL-RX-WP-TP-2009-4051

12. DISTRIBUTION/AVAILABILITY STATEMENT

Approved for public release; distribution unlimited.

13. SUPPLEMENTARY NOTES

To be submitted to Metallurgical Transactions A.

PAO Case Number and clearance date: WPAFB 08-0487, 25 February 2008.

14. ABSTRACT

The chemical partitioning of alloying elements between the disordered y and ordered y' phases in the nickel base superalloy Rene 88DT, has been characterized in detail using three dimensional atom probe tomography (3DAP) coupled with energy-filtered transmission electron microscopy studies. After a homogenization treatment followed by a water quench, it is observed that the morphology of the y' precipitates, reduces with increasing aging time, while the compositional gradient across the y/y' interface decrease. The process of growth of y' precipitates seems to occur through coalescence of adjacent y' precipitates, facilitated through the formation of "necks" between adjacent precipitates. These necks are observed to have intermediate elemental concentration values, between the matrix and the y' precipitate compositions.

15. SUBJECT TERMS

Gamma, Gamma Prime, Nanoscale Characterization, Rene 88DT, Nickel, Superalloy

16. SECURITY CLASSIFICATION OF:			17. LIMITATION OF ABSTRACT:	18. NUMBER OF PAGES	19a. NAME OF RESPONSIBLE PERSON (Monitor)
a. REPORT	b. ABSTRACT	c. THIS PAGE			Christopher F. Woodward
Unclassified	Unclassified	Unclassified	SAR	38	19b. TELEPHONE NUMBER *(Include Area Code)* N/A

Standard Form 298 (Rev. 8-98)
Prescribed by ANSI Std. Z39-18

Nanoscale Characterization of Elemental Partitioning between Gamma and Gamma Prime Phases in Rene 88DT Nickel Base Superalloy

J. Y. Hwang, R. Banerjee, J. Tiley*, R. Srinivasan#, G. B. Viswanathan#, and, H. L. Fraser#

Department of Materials Science and Engineering
University of North Texas, Denton, Texas, U. S. A.

*Materials and Manufacturing Directorate
Air Force Research Laboratory, Dayton, Ohio, U. S. A.

#Department of Materials Science and Engineering
The Ohio State University, Columbus, Ohio, U. S. A.

Abstract

The chemical partitioning of alloying elements between the disordered γ and ordered γ' phases in the nickel base superalloy Rene 88 DT, has been characterized in detail using three dimensional atom probe tomography (3DAP) coupled with energy-filtered transmission electron microscopy studies. After a homogenization treatment followed by a water quench, it is observed that the morphology of the γ' precipitates remains near-spherical even after long aging times. Compositional variation, observed between small (< 5 nm) and larger γ' precipitates, reduces with increasing aging time, while the compositional gradient across the γ/γ' interface decreases. The process of growth of γ' precipitates seems to occur through coalescence of adjacent γ' precipitates, facilitated through the formation of "necks" between adjacent precipitates. These necks are observed to have intermediate elemental concentration values, between the matrix and the γ' precipitate compositions.

Introduction

Ni base superalloys have widespread application in a number of critical technological areas, especially those involving high temperatures. These alloys typically exhibit an excellent balance of properties including good mechanical strength and ductility (both at room and elevated temperatures), improved fracture toughness and fatigue resistance, as well as enhanced creep and oxidation resistance at elevated temperatures. Such a balance of properties makes these alloys suited for application in turbines of jet engines for both aerospace as well as land-based applications. However, with the ever-increasing drive towards more efficient jet engines, there is a continually increasing need for better superalloys capable of withstanding higher temperatures while maintaining the appropriate balance of properties.

Over the past several decades, a number of different nickel base superalloys involving complex chemistries have been developed for aerospace jet engine and land-based gas turbine engine applications, including single crystal alloys for turbine blades and polycrystalline ones for turbine disks. One of the more recent ones is the Rene' 88 DT alloy, that was developed [1-3] to be more damage tolerant than the previous generation Rene' 95 alloy, hence the DT designation, while offering improved creep strength and fatigue crack growth resistance [3]. The nominal chemistry for this alloy is: 13% Co, 16% Cr, 4% MO, 4% W, 2.1% Al, 3.7 % Ti, 0.7% Nb, 0.03% C and 0.015% B. Since Rene 88 DT is an alloy developed for turbine disk applications, it is typically processed through the powder metallurgy route and develops a polycrystalline microstructure

consisting of γ grains with nanoscale γ' precipitates. Furthermore, the typical heat-treatment used for this alloy consists of a solutionizing procedure for 30 to 60 minutes at 1150°C (2100°F) in the γ phase field, followed by cooling to room temperature at appropriate cooling rates, and subsequent aging for different time periods at 760°C (1400°F). Due to the powder processing, a fine γ grain size is achieved within which a duplex distribution of γ' precipitates is formed, the coarser forming on cooling from the single γ phase field (secondary γ'), the finer predominantly on aging (tertiary γ').

The have been a number of studies employing three dimensional atom probe (3DAP) tomography to characterize the atomic scale microstructure of Ni-base superalloys and these studies have been extensively reviewed in recent articles in the published literature [4-6]. The primary emphasis of these studies has been the determination of the size, morphology, and, composition of the γ' precipitates within the γ matrix as a function of the multi-step heat treatments typically experienced by these alloys. In addition, such 3DAP studies have also focused on the partitioning of the alloying additions between these two phases and the segregation of certain alloying additions to interphase (γ/γ' interface) as well as grain boundaries. Of particular interest has been the accurate determination of the compositional profile of different alloying additions across the γ/γ' interface. The overall goal of such studies has been to develop a better understanding of the solute partitioning and its consequent influence on the microstructural evolution process and attendant mechanical properties. However, the upper bound of scale of microstructural features that could be addressed using conventional 3DAP microscopes was severely restricted to typical analysis volumes of approximately 15 x 15 x 100 nm that would often require two days to analyze [7]. With the introduction of the local

electrode atom probe (LEAP) microscope by Imago Inc., it is now possible to achieve analysis rates at least 600 times faster than conventional 3DAP instruments and analysis volumes ~ 100 times larger for the same period of acquisition [4,7].

This paper focuses on the elemental partitioning between γ and γ' phases in Rene' 88 DT as well as on the 3D morphology of the nanoscale γ' precipitates in this alloy. The specific type of heat-treatment considered is solution treatment at 1150°C in the single γ phase field followed by water quenching and subsequently aging at 760°C for different periods of time. The elemental partitioning as well as the 3D morphology have been primarily characterized by 3DAP tomography and complemented with energy-filtered transmission electron microscopy (EFTEM) studies. The three primary objectives of this paper are as follows:

1. A detailed investigation of the elemental partitioning between the γ and γ' phases in this complex alloy containing large number of alloying additions as a function of different different ageing time periods (at 760°C) post a high temperature homogenization treatment.
2. Study of the three-dimensional morphology of the γ' precipitates as a function of ageing time by coupling three-dimensional atom probe (3DAP) tomography with scanning transmission electron microscopy (STEM). Investigate the process of coalescence of γ' precipitates during growth and coarsening.
3. Study of the compositional gradient across the γ / γ' interface as a function of ageing time.

Experimental Procedure

The bulk chemical composition of the commercially procured Rene' 88 DT alloy was 56.53Ni-16.24Cr-13.27Co-3.92Ti-2.09Al-4.08Mo-3.92W-0.76Nb (wt%) or 55.63Ni-18.02Cr-13.00Co-4.74Ti-4.45Al-2.48Mo-1.21W-0.46Nb (at%). Material was cut from the bore and rim section of a turbine disk, produced and tested under a DARPA program [8]. The samples were solution treated at 1150°C in the single γ phase field for 30 minutes to dissolve primary γ' and then water quenched. They were then drilled to accommodate a thermocouple directly in the center of the sample. These samples were subsequently aged for 0, 50, and, 100 hours at 760°C in a large chamber vacuum furnace and air quenched. For convenience, these samples will be subsequently be referred to as WQ0, WQ50, and, WQ100 samples in the remaining part of this paper.

Samples for 3DAP tomography studies in the LEAP microscope were prepared by a combination of electro-polishing and focused ion beam milling techniques. For this purpose, samples from the different heat-treated conditions were first electro-discharge machined into thin wires with a square cross section (~ 0.5 x 0.5 mm). These wires were mechanically ground and subsequently electro-polished to tip diameters ~ 1 μm using a commercially available Electropointer™ system. The electro-polishing was carried out in two steps, first with a 95% acetic acid + 5% perchloric acid solution using 25 V for the coarser polish and finally with an 98% butyl cellulose + 2% perchloric acid solution using 10V for the final polish. These electro-polished needles were subsequently thinned further in a dual-beam focused ion beam (FIB) instrument (FEI Nova Nanolab 200)

system using a Ga ion beam. The ion beam thinning was carried out in multiple steps, starting with 30 kV ions and finally finishing with 5 kV ions to reduce the surface damage caused by the higher energy ions [9]. The final tip diameter of the atom probe specimens was ~ 50 – 80 nm. The 3DAP experiments were carried out using a LEAP 3000 local electrode atom probe (LEAP™) system from Imago Scientific Instruments Inc. All atom probe experiments were carried out in the electric-field evaporation mode at a temperature of 70K, with the evaporation rate varying from 0.2 – 1.0 % and the pulsing voltage at 30% of the steady-state applied voltage.

TEM samples were also prepared via conventional routes, consisting of mechanical grinding and polishing of 3 mm diameter discs, followed by dimple grinding, and, final ion-beam milling to electron transparency. Ion beam milling was conducted on a Gatan Duo Mill and Fischione Model 1010 ion milling system, operated at 6 kV. TEM analysis was conducted on a FEI Tecnai F20 field emission gun transmission electron microscope operating at 200 KV. Images were obtained using the Cr M-edge in the energy filtered transmission electron microscopy (EFTEM) mode, as described elsewhere [10]. Representative regions were imaged at different magnifications to capture the relevant secondary and/or tertiary γ' precipitates in the alloy.

Results

Energy-filtered TEM images, acquired using the Cr M-edge for the water quenched WQ0 sample (without any additional aging) are shown in Figs. 1(a) and (b). The regions

exhibiting a darker contrast in these images, arising from Cr depletion, correspond to the γ' precipitates in the water-quenched condition. These precipitates appear to exhibit a near spherical morphology with a tendency towards flattening of the edges with coarsening. Thus, the relatively larger γ' precipitates exhibit more flattened edges as compared to the smaller precipitates. Another relevant observation is that the contrast in these γ' precipitates appears to vary quite substantially. While this has not been quantified, on a qualitative basis it is clear from Fig. 1(a), that the smaller γ' precipitates appear lighter than the larger precipitates. Unfortunately, due to the two-dimensional nature of these EFTEM images the influence of TEM foil thickness on the contrast exhibited by these γ' precipitates becomes rather convoluted. For example, it is difficult to differentiate between a true compositional difference associated with the smaller γ' precipitates versus an artifact arising from the fact that the smaller precipitates are embedded within the TEM foil and consequently, the contrast visible in the image is a result of averaging between the γ matrix and the γ' precipitate. Therefore, it is critical to determine the true three-dimensional nature of the morphology of these precipitates and also their compositions.

3DAP tomographic reconstructions from the WQ0 sample are shown in Fig. 2. The size of the reconstruction in this case is 35 nm x 35 nm x 110 nm. The red Al-rich regions in Fig.2(a) correspond to the γ' precipitates (since Al preferentially segregates to the γ' phase), while the Co-rich blue regions correspond to the γ matrix. Al=8 at.% isosurfaces, as shown in Fig.2(b), help to delineate the γ' precipitates better. Two different perspective views of the isosurfaces for Cr with threshold values of 14 at% are shown in

Figs. 2(c) and (d). The Cr isosurface views also allow for a clear delineation of the γ' precipitates in the γ matrix. As discussed later, the concentration values for both Al and Cr isosurfaces was selected as the average value between those of the γ' and γ phases for this sample, determined from compositional profiles across the γ'/γ interfaces. The 3D morphology of the γ' precipitates appears to be near-spherical, in agreement with the results of the 2D EFTEM images. The tendency of flattening of the γ'/γ interfaces for the larger precipitates is clearly visible. The overall composition for the entire 3DAP reconstruction for the WQ0 sample is listed in Table I. The average compositions of the γ and γ' phases for this reconstruction have also been listed in the same table. Note that the composition of the γ' phase listed in Table I is an average value for ~ 15 individual precipitates measured in the 3DAP reconstruction shown in Fig. 2. The individual compositions of 4 of these γ' precipitates have been listed in Table II together with the associated error bars in the measurement. Amongst the four γ' precipitates, γ'1 and γ'2 are relatively larger in size with equivalent diameters greater than 5 nm while γ'3 and γ'4 are relatively small in size with equivalent diameters ~3 nm. Comparing the compositions of these four precipitates, it is apparent that while γ'1 and γ'2 exhibit similar compositions, the compositions of smaller γ'3 and γ'4 are significantly different, especially with respect to certain alloying additions. Thus, concentrations of Co, Cr, and, Mo are marginally higher while the Al content is marginally lower in case of γ'3 and γ'4 as compared to γ'1 and γ'2. These results are rather interesting, indicating the partitioning tendencies of different alloying additions during the early stages of γ' precipitation. The compositional profile across the γ'/γ interfaces for the WQ0 sample has been determined

using a powerful analysis tool, the proximity histogram (proxigram in short) [11] for the various γ' precipitates, visible in the reconstructions shown in Figs. 2(c) and (d). These proxigrams can be used for any internal surface, even those involving a complex topology. The ones discussed in the present study are all for internal interfaces constructed based on isosurfaces with a threshold value of Cr = 14 at%. For example, a typical proxigram for one specific γ' precipitate is shown in Fig. 3(a). The figure on the left of Fig. 3(a) shows a section of the overall reconstruction with the specific γ' precipitate marked. The proxigram for this specific precipitate is shown on the right of the same figure with the error bars included for the different alloying additions. In this case only the primary alloying elements, Cr, Co, Mo, Al, and, Ti, have been included in the plot. As expected,the partitioning of the alloying additions involves preferential segregation of Al and Ti to the γ' phase while the γ phase is enriched in Cr, Co, and, Mo. It should be noted that the Mo segregation is rather limited with the γ phase exhibiting only a marginally higher Mo content as compared to the γ' phase. An additional feature to note in the 3DAP reconstructions shown in Figs. 2(c) and (d) is that in some cases, two (or more) γ' precipitates appear to be connected by necks during the process of coalescence during growth. Higher magnification views of such necks between γ' precipitates and the corresponding compositional profiles are shown in Figs. 3(b) and (c). The compositional profiles in each of these figures correspond to the respective cylinders shown in the 3DAP reconstructions. However, it should be noted that for the sake for better visualization, the length of the cylinder is larger than the length of the plotted compositional profile. Fig. 3(b) shows two γ' precipitates separated by a relatively thin neck region with the composition of this neck region lying in between that of the

adjoining γ' precipitates and the γ matrix. Thus, while the Cr, Co, and, Mo content of the neck region is higher than the adjoining γ' precipitates, the Al and Ti contents are lower. Similarly, the Co, Cr, and, Mo content in the neck region is lower than that in the γ matrix. The situation is different in case of the neck shown in Fig. 3(c). In this case, the composition of the neck region is virtually indistinguishable from that of the adjoining γ' precipitates with possibly a very small increase in the Cr and Co content. This may indicate a case where the neck has indeed reached the stable composition of the γ' precipitate.

An EFTEM image from the WQ50 sample (aged at 760°C for 50 hours), recorded using the Cr M-edge is shown in Fig. 4. The γ' precipitates, exhibiting the darker contrast, appear coarser than those observed in the WQ0 sample [12]. Furthermore, there are distinct neck regions, forming between adjoining γ' precipitates, visible in this EFTEM image (Fig. 4(a)). Intensity line profiles across a couple of these necks, marked A-B and C-D, are shown in Figs. 4(b) and (c) respectively. Such intensity profiles can be used as qualitative indicators of the Cr content variation across the γ-γ' interface. Thus, in case of the A-B neck, it can be inferred from Fig. 4(b) that the Cr content is higher in the neck region as compared to that in the adjoining γ' precipitates. In contrast, in case of the C-D neck, Fig. 4(c) shows a virtually indistinguishable neck region without any significant difference in the composition between the neck and the adjoining γ' precipitates (as for the case shown in Fig.3(c)). Furthermore, Fig. 4(b) also shows an intermediate intensity for the neck region, implying that the Cr content of the neck region, while higher than that of the adjoining γ' precipitates, is still lower than that in the γ matrix. Again, while

such intensity profiles are promising ways to analyze the composition, the complexities introduced due to variations in foil thickness and associated averaging of the compositional data cannot be neglected. Detailed 3DAP analysis does not suffer from such ambiguities. 3DAP reconstructions from the WQ50 sample are shown in a series of images in Fig. 5. The size of the reconstruction in this case is 70 nm x 70 nm x 70 nm. Fig. 5(a) shows the Al ions in red and Co ions in blue, while Fig. 5(b) shows Al = 8 at% iso-concentration surfaces (isosurfaces) in red together with the Co ions in blue. Two different perspective views of the isosurfaces for Cr = 14 at% are shown in Figs. 5(c) and (d). Comparing the size of the γ' precipitates in this case with the WQ0 sample, it appears that the average size of the precipitates is larger in the WQ50 sample. However, since there are only a limited number of γ' precipitates captured in the 3DAP reconstruction, it is somewhat difficult to comment on quantitative values of average sizes based on such limited numbers (note that EFTEM micrographs provide a good complementary tool for this purpose, as the area analyzed through EFTEM is considerably larger [12]). The 3D morphology of the γ' precipitates appears to be near-spherical with necks forming as adjoining γ' precipitates coarsen. The overall composition for the entire 3DAP reconstruction for the WQ50 sample is listed in Table III. The average compositions of the γ and γ' phases for this reconstruction have also been listed in the same table. No significant differences were observed between the compositions of individual γ' precipitates after 50 hours of aging at 760°C. An interface proxigram for one of the γ' precipitates in the 3DAP reconstruction has been shown in Fig. 6(a). The partitioning trends are similar to those observed for the case of the WQ0 sample, and also consistent with expectations with Co, Cr, and, Mo partitioning preferentially to the γ matrix while

the Al and Ti partition to the γ' precipitates. An analysis of the neck region formed between two adjacent coarsening γ' precipitates is shown in Figs. 6(b) and (c). Thus, the specific compositional profile across the same neck is shown for two nearly perpendicular directions in these two figures. The profile across the two γ' precipitates and the neck in between is shown in Fig. 6(b), with the neck region exhibiting higher contents of Cr, Co, and Mo, and lower contents of Al and Ti as compared with the γ' precipitates. In contrast, the profile across the same neck region along a nearly perpendicular direction, going from γ matrix to neck to γ matrix (as clearly represented by the cylinders in the Cr isosurface reconstructions), is shown in Fig. 6(c). From this profile it is apparent that the neck region has a lower Cr, Co, and Mo content as compared to the adjoining γ matrix. Based on these observations it can be concluded that the composition of this neck lies in between that of the γ' precipitates and the surrounding γ matrix, consistent with the deductions from the intensity profiles across the A-B neck region, shown in the Cr EFTEM image in Fig. 5.

Finally, an EFTEM image of the γ' precipitates in the WQ100 sample is shown in Fig. 7(a) together with intensity line profiles in Figs. 7(b) - (d). Fig. 7(b) shows the intensity profile across the E-F line marked in Fig. 7(a), across γ / γ' / γ interfaces. Significantly lower intensity is observed within the γ' precipitate in this case. Figs. 7(c) and (d) show intensity profiles across the neck regions, A-B and B-C, marked in Fig. 7(a). In both these profiles, an increase in intensity in the neck region is distinctly visible, again indicating that the Cr content in the neck region is higher as compared to the adjoining γ' precipitates. A comparison of the intensity within the γ matrix to that within the neck

region (both relative to the γ' precipitates), shows that the Cr content in the neck region is presumably lower than that in the γ matrix. Interestingly, the absolute intensity level observed within the γ' precipitate can also be used as a means of qualitatively assessing the precipitate size, and consequently, an estimate of the volume fraction can be obtained [10]. 3DAP reconstructions from the WQ100 sample are shown in a series of images in Fig. 8. The size of the reconstruction in this case is 50 nm x 50 nm x 41 nm. Fig. 8(a) shows the Al ions in red and Co ions in blue, while Fig. 8(b) shows Al = 8 at% iso-concentration surfaces (isosurfaces) in red together with the Co ions in blue. Two different perspective views of the isosurfaces for Cr = 14 at%, shown in Figs. 8(c) and (d), clearly indicate the tendency of the γ' precipitates to coalesce by forming necks during the process of coarsening. The overall composition for the entire 3DAP reconstruction, including the compositions for the γ and γ' phases, for the WQ100 sample are listed in Table IV. No significant differences were observed between the compositions of individual γ' precipitates after 100 hours of ageing at 760°C. An interface proxigram for one of the γ' precipitates in the 3DAP reconstruction, together with the actual reconstruction with the particular precipitate marked, are shown in Fig. 9. The partitioning trends are similar to those observed in case of the WQ0 and WQ50 samples.

Discussion

A comparison of the 3DAP results for all the three different heat treated conditions, WQ0, WQ50, and, WQ100, allows for a better understanding of the microstructural

evolution in the Rene 88 DT alloy. As expected, the finest scale of γ' precipitates was observed in the directly water-quenched WQ0 sample. The near-spherical morphology of these precipitates, observed in case of the 3DAP reconstruction, is in good agreement with the 2D morphology observed in case of the Cr EFTEM images. Such a morphology is expected in case of the Rene 88DT alloy considering the relatively small (~ 0.05%) positive misfit between the γ' precipitates and the γ matrix [3]. The small misfit value is also likely to lead to a near-spherical morphology of precipitates even when they coarsen to larger sizes, due to the relatively minor role of strain energy. On ageing for 50 hrs or 100 hrs at 760°C, the γ' precipitates coarsen, with a tendency for flattening of the γ/γ' interfaces, presumably due to the increasing strain energy associated with these precipitates.

Interestingly, the composition of the γ' precipitates exhibits a wide spread in case of the WQ0 sample, presumably due to the fact that these precipitates are in the early stages of their growth and have not yet reached an equilibrium composition. More importantly, the smaller the size of the γ' precipitate, the further its composition is found to be from the expected equilibrium composition. Such compositional differences between different γ' precipitates are substantially reduced after aging for 50 or 100 hrs at 760°C. A comparison of the average compositions of the γ' precipitates together with the spread between different precipitates for the WQ0, WQ50, and, WQ100 samples has been shown in the form of a bar chart in Fig. 10. From this chart, it is apparent that for almost all the alloying elements in Rene 88 DT, the maximum spread in composition between different γ' precipitates is observed for the WQ0 sample. With increasing aging time at

760°C, the compositional spread between different γ' precipitates appears to gradutally decrease, with the WQ50 and WQ100 samples exhibiting progressively smaller compositional spreads. It should be noted that the maximum decrease in the compositional spread is observed on comparing WQ50 and WQ0 samples suggesting that *the γ' precipitates are likely to achieve their stable composition, close to equilibrium, within the first 50 hours of aging*. Furthermore, while the compositional spread between the γ' precipitates decreases on ageing, the average composition of the γ' phase remains the same for the WQ0, WQ50, and, WQ100 samples (refer to Fig. 10). The small changes between these three ageing times, visible in Fig. 10, are probably not statistically significant considering the rather limited volume of material sampled in the 3DAP reconstructions. Similarly, comparing the composition of γ matrix for these three samples (from Tables I, III, and, IV), it is evident that with increasing ageing time, this composition approaches a stable value. In this case too, the difference between the γ compositions of the WQ0 and WQ50 samples is substantially greate15 than the difference between the WQ50 and WQ100 samples. These trends in the compositional changes within the γ matrix (as a function of aging time) clearly indicate that for aging at 760°C between 0 to 50 hrs, the undersaturation of alloying additions such as Co, Cr, and, Mo, and supersaturation of alloying additions such as Ti and Al, is removed and consequently γ' precipitate dynamics transitions from the predominantly growth to the predominantly coarsening (or coalescing) regime of the transformation.

During the coarsening of the γ' precipitates, coalescence of adjacent precipitates is often observed as clearly visible in case of all the EFTEM images and the 3DAP

reconstructions for WQ0, WQ50, and, WQ100 samples, discussed in this paper. The coalescence of these precipitates can possibly proceed via the formation of necks that facilitate the coalescence. The composition of the neck region, determined using 3DAP, has an intermediate value between the γ' precipitate and the adjoining γ matrix compositions, at least during the early stages of the coalescence process. The same result is qualitatively corroborated by the Cr-EFTEM maps in which case the neck regions exhibit a contrast that is brighter than the adjacent γ' precipitates and darker than the γ matrix. Previous work by Yoon et. al. [13] clearly shows that the neck regions between γ' precipitates exhibit long range $L1_2$ ordering. Therefore, it appears that during coarsening of the γ' precipitates, the neck regions formed between coalescing precipitates, become structurally ordered prior to achieving stable composition. However, more detailed studies are required in order to understand the factors that drive the formation of necks that cause γ' coarsening; specifically, the role of precipitate morphology and existing precipitate composition (at the time of neck formation) need further exploration.

The compositional gradient across the γ/γ' interface can be approximately estimated from the proximity histograms for the different aging times, representative samples of which are shown in Figs. 3(a), 6(a), and, 9 for the WQ0, WQ50, and, WQ100 samples respectively. The average width of the compositional gradients corresponding to the WQ0, WQ50, and, WQ100 samples are 2.2 nm, 3.1 nm, and, 3.1 nm respectively. For each sample, the width of the compositional gradient has been calculated based on an average of three different proxigrams (corresponding to three different γ' precipitates). While these values of compositional widths can be used as qualitative guidelines, it is

important to realize that the X-axis in the proxigrams shown in Figs. 3(a), 6(a), and, 9 does not strictly correspond to a linear distance scale, but more appropriately to proximity to the interface [11]. Thus, while this distance is more representative of a linear distance in case of planar γ/γ' interfaces, the situation can change as the interface becomes more curved and complex in shape. Nevertheless, comparing the three proxigrams, it is rather interesting that the compositional gradient appears to decrease with increasing ageing time in these samples with the sharpest gradient appearing in case of the WQ0 sample. The underlying thermodynamic rationale behind the decrease in the compositional gradient across the interface (with increasing ageing time) needs further detailed analysis. Additionally, the implications of the effect of observed compositional gradient on the ensuing features (such as misfit and dislocation substructures created during deformation), need to be carefully explored.

Summary and Conclusions

The compositional partitioning of alloying additions together with the 3D morphological evolution associated with the precipitation of γ' within the γ matrix of a commercial Rene 88DT alloy have been studied as a function of ageing time primarily using 3DAP tomography. Both 3DAP data as well as Cr-EFTEM images of these γ' precipitates indicate that their morphology is near-spherical with some flattening of the γ/γ' interfaces occurring during precipitate coarsening. During the initial stages of γ' precipitation, in the WQ0 (directly water quenched sample) the partitioning of the alloying elements is incomplete in case of the smaller precipitate sizes (~ 3 nm) while the coarser γ'

precipitates (> 5 nm) exhibit compositions close to the equilibrium values. The spread in the compositions of the γ' precipitates reduces substantially with increasing ageing time and is minimal after ageing for 100 hrs at 760°C. The compositional gradient across the γ/γ' interface decreases with increasing ageing time, with the width increasing from ~ 2.2 nm in case of the WQ0 sample to ~ 3.1 nm for the WQ50 and WQ100 samples. Finally, during the coarsening and coalescence of the γ' precipitates, necks are formed between adjoining precipitates and the local composition in the neck region (~ 2 – 3 nm in diameter), measured using 3DAP tomography, lies in between that of the adjoining γ' precipitates and the γ matrix.

Acknowledgements

The authors would like to acknowledge the U. S. Air Force Office of Scientific Research (AFOSR Grant # FA9550-06-1-0193) for providing financial support for this study. In addition, the authors also gratefully acknowledge the Center for Advanced Research and Technology (CART) at the University of North Texas and the Center for the Accelerated Maturation of Materials (CAMM) at the Ohio State University for access to the experimental facilities used for this study.

References

1. D. D. Krueger, R. D. Kissinger, R. D. Menzies, and, C. S. Wukusick, *U. S. Patent* 4,957,567.
2. D. D. Krueger, R. D. Kissinger, and, R. D. Menzies, *Superalloys 1992*, Ed. S. D. Antolovich et. al., TMS-AIME, Warrendale, PA, 277-286 (1992).
3. S. T. Wlodek, M. Kelly, and, D. A. Alden, *Superalloys 1996*, Ed. R. D. Kissinger, D. J. Deye, D. L. Anton, A. D. Cetel, M. V. Nathal, T. M. Pollock, and, D. A. Woodford, TMS, Warrendale, PA, 129-136 (1996).

4. D. N. Seidman, C. K. Sudbrack, and, K. E. Yoon, *JOM*, December 2006.
5. M. K. Miller, *Micron*, **32**, 757 – 764 (2001).
6. D. Blavette, E. Cadel, and, B. Deconihout, *Mater. Charac.*, **44**, 133-157 (2000).
7. S. S. A. L. Gerstl, D. N. Seidman, A. A. Gribb, and, T. F. Kelly, *Advanced Materials and Processes*, p. 31, October 2004.
8. DARPA program reference.
9. K. Thompson, D. Lawrence, D. J. Larson, J. D. Olson, T. F. Kelly, and, B. Gorman, *Ultramicroscopy*, **107**, 131 (2007).
10. P. M. Sarosi, G. B. Viswanathan, D. Whitis, and, M. J. Mills, Ultramicroscopy, 103, 83-93 (2005).
11. O. C. Hellman, J. A. Vandenbroucke, J. Rusing, D. Isheim, and, D. N. Seidman, *Micros. Microanal.*, **6**, 437-444 (2000).
12. J. Tiley, G.B. Viswanathan, R. Srinivasan, R. Banerjee, H.L. Fraser, in preparation.
13. K. E. Yoon, C. K. Sudbrack, R. D. Noebe, and, D. N. Seidman, Z. Metallkund., 5, 481-485 (2005).

Tables

	Bulk		γ	γ' (avg)
	Atomic%	Error%	Atomic%	Atomic%
Ni	48.96	0.05	46.10	58.07
Co	12.89	0.02	14.30	8.83
Ti	4.69	0.01	2.50	10.67
Cr	18.92	0.03	23.50	4.68
Al	6.13	0.02	4.20	10.49
Nb	2.32	0.01	2.30	2.97
Mo	4.24	0.01	4.80	3.29
C	0.09	0.00	0.10	0.07
W	1.61	0.01	2.00	1.26
B	0.15	0.00	0.20	0.14

Table I: The bulk (overall 3DAP reconstruction), γ, and, average γ' compositions for the WQ0 sample.

	γ'1		γ'2		γ'3		γ'4	
	Atomic%	Error%	Atomic%	Error%	Atomic%	Error%	Atomic%	Error%
Ni	59.62	0.65	59.34	0.72	57.10	1.67	51.00	1.92
Co	7.69	0.19	7.45	0.21	10.90	1.05	13.80	1.33
Ti	10.85	0.23	10.90	0.26	10.14	1.02	13.10	1.30
Cr	4.21	0.14	4.06	0.15	5.50	0.77	6.20	0.93
Al	10.55	0.23	11.06	0.26	8.30	0.93	9.70	1.14
Nb	2.72	0.11	2.86	0.13	2.10	0.48	7.00	0.98
Mo	2.86	0.11	2.88	0.13	3.60	0.63	4.10	0.76
C	0.04	0.01	0.07	0.02	0.20	0.15	0.00	0.00
W	1.32	0.08	1.25	0.08	1.90	0.46	1.40	0.45
B	0.13	0.02	0.12	0.03	0.00	0.00	0.00	0.00

Table II: The compositions of individual γ' precipitates of different sizes in the WQ0 sample. γ'1 and γ'2 are larger sized (> 5 nm) precipitates while γ'3 and γ'4 are smaller sized precipitates.

	Bulk		γ	γ'
	Atomic%	Error%	Atomic%	Atomic%
Ni	48.08	0.03	40.00	59.51
Co	13.86	0.01	17.40	7.93
Ti	4.32	0.01	0.80	10.44
Cr	19.41	0.02	30.10	3.32
Al	5.99	0.01	2.90	11.35
Nb	2.38	0.01	1.90	2.95
Mo	4.33	0.01	5.20	3.09
C	0.06	0.00	0.10	0.06
W	1.45	0.00	1.50	1.24
B	0.11	0.00	0.10	0.12

Table III: The bulk (overall 3DAP reconstruction), γ, and, average γ' compositions for the WQ50 sample.

	Bulk		γ	γ'
	Atomic%	Error%	Atomic%	Atomic%
Ni	46.65	0.05	41.10	57.13
Co	15.38	0.03	18.20	8.81
Ti	3.52	0.01	0.80	9.97
Cr	19.59	0.03	27.00	3.52
Al	5.04	0.01	2.50	10.84
Nb	2.38	0.01	2.00	3.09
Mo	5.43	0.02	5.70	4.62
C	0.06	0.00	0.10	0.05
W	1.85	0.01	1.90	1.88
B	0.09	0.00	0.10	0.09

Table IV: The bulk (overall 3DAP reconstruction), γ, and, average γ' compositions for the WQ100 sample.

Figure Captions

Fig. 1(a) and (b) Energy-filtered TEM (EFTEM) images constructed using the Cr M-edge in the EELS spectrum from the solutionized and water-quenched (WQ0) sample. The γ' precipitates, which are Cr depleted, exhibit the darker grey contrast in these images.

Fig. 2(a) 3DAP reconstruction of the Co (blue) and Al (red) atoms in the WQ0 atom probe sample. The γ' precipitates are the Al-rich red regions within the Co-rich blue matrix (b) A different depiction of the same 3D reconstruction showing Co atoms in blue and isoconcentration surfaces (isosufaces) for Al = 8 at% in red. Such a depictions permits for a more clearer visualization of the γ' precipitates. (c) and (d) Two different perspective views of the 3D reconstruction for the WQ0 sample showing Cr = 14 at% isosurfaces. Note the near spherical morphology of the γ' precipitates with a tendency for formation of flattened interfaces as the γ' precipitates become larger in size. Also, note the formation of nanometer scale necks forming in between the γ' precipitates.

Fig. 3(a) Proximity histogram for a specific γ' precipitate (shown shaded in the 3D reconstruction on the left), exhibiting the clear partitioning of the alloying elements between the γ (right side of the interface) and γ'(left side of the interface) phases. Note the width of the compositional gradient across the γ/γ' interface. (b) The compositional profile along the axis of a cylinder of diameter 5 nm, aligned across a necked region between two distinctly different γ' precipitates. Note that the composition of the neck region lies in between that of the γ and γ'phases. (c) Compositional profile across a different neck in the same 3D reconstruction from the WQ0 sample.

Fig. 4(a) Cr EFTEM image from the sample aged at 760°C for 50 hours (WQ50) sample. The γ' precipitates, which are Cr depleted, exhibit the darker grey contrast in these images. (b) Intensity line profile across the line marked AB in (a). The neck region exhibits an intensity lying in between that of the γ and γ'phases. (c) Intensity profile across the line CD in (a). The necked region in this case does not appear to exhibit any difference in intensity from that of the adjoining γ'precipitates.

Fig. 5(a) 3DAP reconstruction of the Co (blue) and Al (red) atoms in the WQ50 sample. (b) A different depiction of the same 3D reconstruction showing Co atoms in blue and isoconcentration surfaces (isosufaces) for Al = 8 at% in red. (c) and (d) Two different perspective views of the 3D reconstruction for the WQ0 sample showing Cr = 14 at% isosurfaces.

Fig. 6(a) Proximity histogram for a specific γ' precipitate (shown shaded in the 3D reconstruction on the left), exhibiting the clear partitioning of the alloying elements between the γ (right side of the interface) and γ'(left side of the interface) phases in the WQ50 sample. (b) The compositional profile along the axis of a cylinder of diameter 5 nm, aligned across a necked region between two distinctly different γ' precipitates. Note that the composition of the neck region lies in between that of the γ and γ'phases. (c)

Compositional profile across the same neck, along a cylinder aligned perpendicular to the original one shown in (b) for the WQ50 sample.

Fig. 7 (a) Cr EFTEM image from the sample aged at 760°C for 100 hours (WQ100) sample. The γ' precipitates, which are Cr depleted, exhibit the darker grey contrast in these images. (b) Intensity line profile across the line marked EF in (a) across a single γ' precipitate. (c) Intensity line profile across the line marked AB in (a). The neck region exhibits an intensity lying in between that of the γ and γ'phases. (d) Intensity profile across the line BC in (a). The neck region exhibits an intensity lying in between that of the γ and γ'phases.

Fig. 8(a) 3DAP reconstruction of the Co (blue) and Al (red) atoms in the WQ100 sample. (b) A different depiction of the same 3D reconstruction showing Co atoms in blue and isoconcentration surfaces (isosufaces) for Al = 8 at% in red. (c) and (d) Two different perspective views of the 3D reconstruction for the WQ0 sample showing Cr = 14 at% isosurfaces.

Fig. 9 Proximity histogram for a specific γ' precipitate (shown shaded in the 3D reconstruction on the left), exhibiting the clear partitioning of the alloying elements between the γ (right side of the interface) and γ'(left side of the interface) phases in the WQ100 sample. Note the relatively large width of the compositional gradient across the interface.

Fig. 10. Bar chart comparing the compositions of the γ' precipitates for all the three samples, WQ0, WQ50, and, WQ100. The height of the bars correspond to the average composition of the γ' phase while the spread in compositions marked on each bar corresponds to the compositional spread between different γ' precipitates within the same sample.

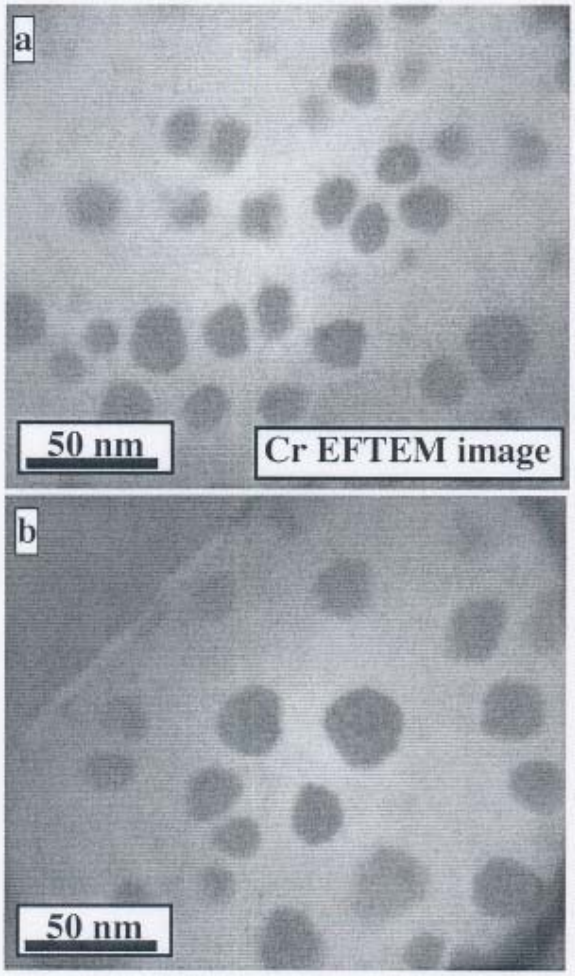
a
50 nm
Cr EFTEM image
b
50 nm

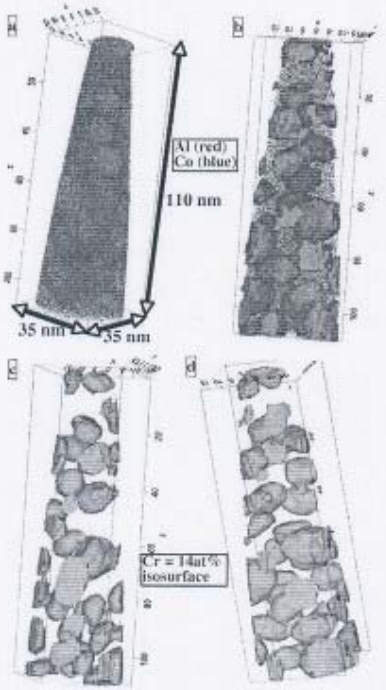
Al (red)
Co (blue)
110 nm
35 nm
35 nm
Cr = 14at%
isosurface

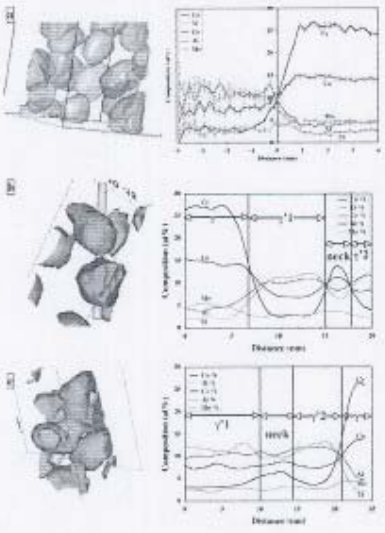

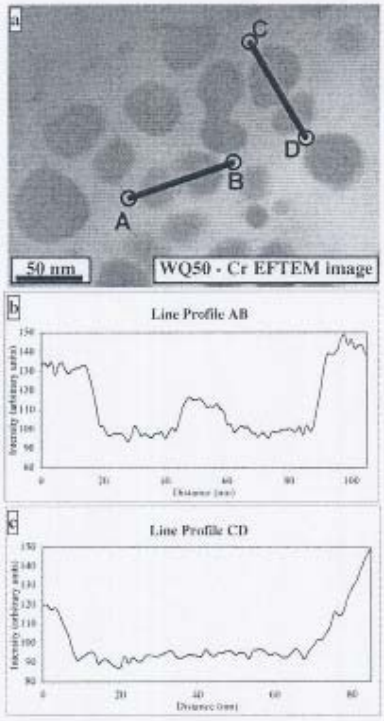
a
C
D
B
A
50 nm
WQ50 - Cr EFTEM image
b
Line Profile AB
c
Line Profile CD

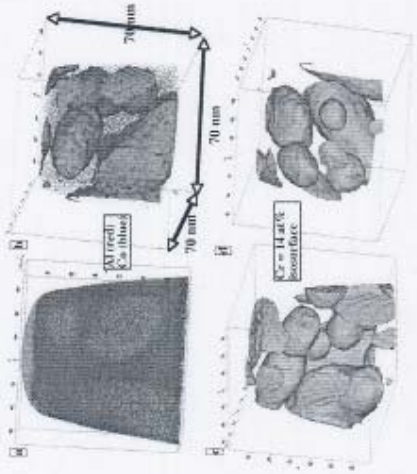
70 mm
70 mm
70 mm

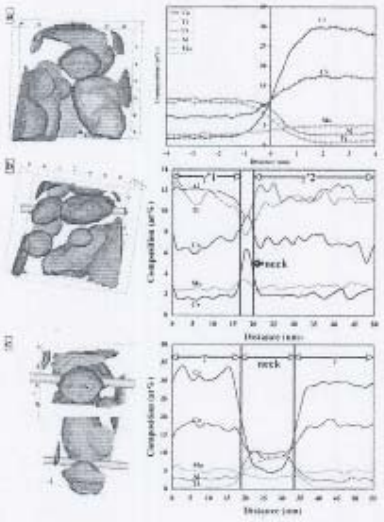
A
B
C
neck
neck

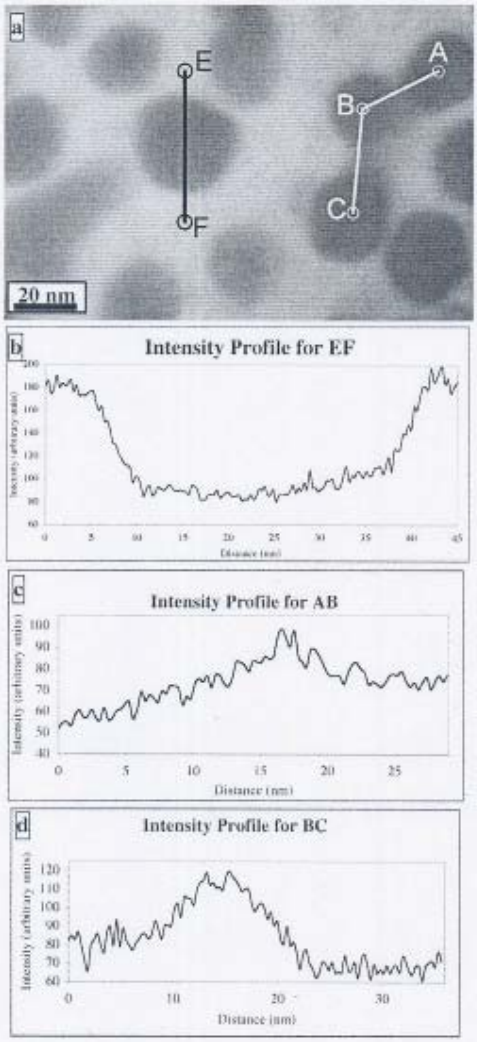
a
E
F
A
B
C
20 nm
b
Intensity Profile for EF
c
Intensity Profile for AB
Intensity (arbitrary units)
Distance (nm)
d
Intensity Profile for BC
Intensity (arbitrary units)
Distance (nm)

50 nm
50 nm
41 nm

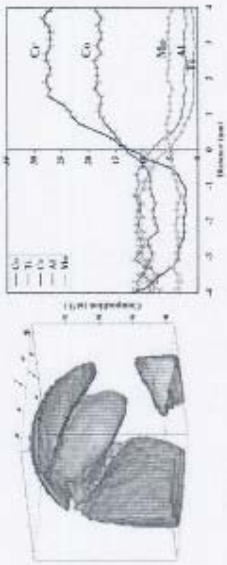

WQ0
WQ50
WQ100
0.7000
0.6000
0.5000
0.4000
0.3000
0.2000
0.1000
0.0000
Composition (atomic frac)
Ni
Co
Ti
Cr
Al
Nb
Mo